



**HAL**  
open science

## Soft ferrite cores characterization for integrated micro-inductors

Yen Mai Nguyen, David Bourrier, Samuel Charlot, Zarel Valdez Nava, Vincent Bley, Céline Combettes, Thomas Lopez, Jean-Pierre Laur, Magali Brunet

► **To cite this version:**

Yen Mai Nguyen, David Bourrier, Samuel Charlot, Zarel Valdez Nava, Vincent Bley, et al.. Soft ferrite cores characterization for integrated micro-inductors. *Journal of Micromechanics and Microengineering*, 2014, 24 (10), 10.1088/0960-1317/24/10/104003 . hal-01443220

**HAL Id: hal-01443220**

**<https://hal.science/hal-01443220>**

Submitted on 13 Mar 2018

**HAL** is a multi-disciplinary open access archive for the deposit and dissemination of scientific research documents, whether they are published or not. The documents may come from teaching and research institutions in France or abroad, or from public or private research centers.

L'archive ouverte pluridisciplinaire **HAL**, est destinée au dépôt et à la diffusion de documents scientifiques de niveau recherche, publiés ou non, émanant des établissements d'enseignement et de recherche français ou étrangers, des laboratoires publics ou privés.

# Soft ferrite cores characterization for integrated micro-inductors

Yen Mai Nguyen<sup>1,3</sup>, David Bourrier<sup>1,3</sup>, Samuel Charlot<sup>1,3</sup>, Zarel Valdez-Nava<sup>2,3</sup>, Vincent Bley<sup>2,3</sup>, Céline Combettes<sup>2,3</sup>, Thomas Lopez<sup>1</sup>, Jean-Pierre Laur<sup>1,3</sup>, Magali Brunet<sup>1,3</sup>

<sup>1</sup>CNRS, LAAS, 7 avenue colonel Roche, F-31400 Toulouse, France

<sup>2</sup>CNRS, LAPLACE, 118 route de Narbonne, F-31062 Toulouse, France

<sup>3</sup>Université de Toulouse; UPS, INPT; LAAS, LAPLACE, Toulouse, France

Email: mbrunet@laas.fr

## Abstract

Low profile soft ferrite films constitute a competitive solution for the integration of micro-inductors on silicon in low-power medium frequency DC-DC conversion applications. High resistivity of soft ferrites is indeed a major advantage for operating frequencies in the range of 5-10 MHz. We have studied several soft ferrites including commercial ferrite films and in-house made ferrites. Test inductors were fabricated at wafer level using micromachining and assembling techniques. The proposed process is based on a sintered ferrite core placed in between thick electroplated copper windings. The low profile ferrite cores of  $1.2 \times 2.6 \times 0.1$  mm<sup>3</sup> were produced by two methods issued from green tape-casted films or ferrite powders. This article presents the magnetic characterization of the fabricated ferrite cores cut and printed in rectangular shape and sintered at different temperatures. The comparison is made in order to find out the best material for the core that can offer the micro-inductor a high inductance in the range of 200-1000 nH at 6 MHz and that generate the smallest losses. With commercial ferrite core, it is demonstrated, thanks to a test inductor, that an inductance density of 215 nH.mm<sup>-2</sup> up to 6 MHz could be reached. Extracted losses at 6 MHz, under 10 mT are in the range of 0.8 to 2.5 W.cm<sup>-3</sup>.

**Key words:** Micro inductor, ferrite, on-chip integration, Power SoC

---

## 1. Introduction

The trend towards miniaturization of mobile electronic products with the demand of improving functionality and performance raises challenges for power management systems for which higher power density with higher energy conversion efficiency is required. In advanced DC-DC converters, the control circuits and power semiconductor devices can be fully integrated but the passive components especially inductors and transformers are still obstacles for further reducing the size of DC-DC converters. A lot of researches have been carried out to achieve inductor integration on-chip or in-package. Some demonstrators of air-core inductors, thin film magnetic inductors, and ferrite based ones have shown that each integration method has its own merit and difficulties [1-15]. For on-chip integration, the approaches to the fabrication of micro-inductors involving vacuum deposition and electro-deposition of magnetic cores have been demonstrated over the last thirty years. Vacuum deposition techniques, i.e. sputtering or evaporation, can be used to deposit a wide range of magnetic materials including alloys and oxides such as Ni-Fe-Zr based, Co-Zr based, Co-Hf-Ta-Pd, Co-Fe-Hf-O, Ni<sub>80</sub>Fe<sub>20</sub>, Fe-B-N or Fe-Co-based amorphous thin films [7,16]. Despite the disadvantage of slow deposition rate, these sputtered materials usually have good soft

magnetic properties: amorphous alloys exhibit typically high induction saturation ( $> 1\text{ T}$ ) and small coercive field (several Oe). On the other hand, oxides have high electrical resistivity which allows characteristics to be maintained up to the GHz range [16]. However, when the film is thicker than several micro-meters, stress can develop in the layer and etching of thick metallic films is an issue. Dry etching of thick films usually involves long etching times resulting in heating of the substrate and degradation of the magnetic film properties while wet etching of thick films results in severe undercutting. Alternatively, sputtered films have been deposited through shadow masks up to tens of microns [17]; however the problem of delamination and cracking still happened for the second layer of deposition due to an unfortunate issue of over-heating within the chamber. Electroplating is a less costly method than vacuum deposition techniques and more suitable for micro-inductor cores with large cross-sectional areas. The films deposited by electroplating have thickness of several micro-meters to several tens of micro-meter including alloys of NiFe with different composition such as  $\text{Ni}_{80}\text{Fe}_{20}$ ,  $\text{Ni}_{45}\text{Fe}_{55}$ ,  $\text{Ni}_{50}\text{Fe}_{50}$  and others like CoFeNiC, CoPFe, CoNiFe, CoFeCu, NiFeMo [11,18,19]. With this technique, only conductive materials can be electroplated; so, due to high frequency operation eddy currents can be considerable and should be controlled by lamination. Recently, laminated thick films of electroplated metallic alloys were demonstrated for CoNiFe with about 40 layers,  $1\ \mu\text{m}$  thick for each layer. The test inductor demonstrated a constant inductance of  $1.6\ \mu\text{H}$  up to 10 MHz, indicating suppressed eddy current losses [12].

Screen printing of ferrite powder or magnetic composites is an alternative approach compared to the two above-mentioned methods [20,21]. It has some fabrication advantages such as fast deposition and much larger achievable thickness up to several hundreds of micro-meter.

In terms of performance, soft ferrite materials present an interesting solution for integration, in particular NiZn ferrites with formula  $\text{Me}_x\text{Ni}_y\text{Zn}_z\text{Fe}_2\text{O}_4$  where Me refers to transition divalent metals with  $x + y + z = 1$ . They are usually employed for realizing bulk inductors and/or LTCC low profile inductors [22,23]. Their high resistivity, in the range of  $10^3\text{-}10^6\ \Omega\cdot\text{m}$  would tend to minimize eddy current losses at high frequencies and the coercive field ranges from less than 1 Oe to several Oe. Losses of NiZn ferrites are in the range of  $100\text{-}1000\ \text{mW}\cdot\text{cm}^{-3}$  at 3 MHz under 10 mT [24]. Besides, their permeability can be relatively high: from tens to hundreds and induction saturation is around 0.20-0.30 T. Composition and microstructure largely influence magnetic properties of NiZn ferrites. Moreover, the ferrite powder needs to be sintered at high temperature (usually about  $900^\circ\text{C}$ ) to achieve desired magnetic properties. Regarding CMOS compatibility, such high temperatures can be a problem for most materials already presented on the substrate but there are some ways to tackle this issue. For integrated ferrite-based micro-inductors, some authors have done sintering of the bottom ferrite layer for spiral-type inductors then completing with a composite top layer [8], some have done sintering of the bottom and top ferrite layer in-situ [25]. Others have developed hybrid solutions where the core is fabricated off-chip [15].

In general, however, ferrite-based inductors reported in literature are either bulky when the core is realized off-chip [4,26], either they don't show optimal performance due to the fact that ferrite material is not sintered or it is mixed with polymer [8,27,28]. In [8] for instance, the magnetic composite layer has low permeability of 25 while the fully-sintered magnetic layer has higher permeability of 120. In the case of the micro-inductors in the toroidal structure reported by Fang [27] the permeability of the non-sintered magnetic composite core (Mn-Zn) is only 5.

Consequently, the fabricated inductor has an inductance of about 40 nH for a foot print of 3 mm<sup>2</sup>, corresponding hence to 15 nH.mm<sup>-2</sup> in density. Micro-inductors with Ni-Zn ferrite composite in spiral and pot-core designs have shown inductance densities about 40 nH.mm<sup>-2</sup> for footprint of 9 and 20 mm<sup>2</sup> respectively [26,28]. With these ferrite/polymer composites, core losses have not been reported.

Thanks to the adequate thickness and pre-eminent magnetic properties, fully-sintered ferrite-based cores offer high inductance densities for the integrated inductors. In our previous works [29,30], we presented a possible solution for integrating very small size (< 4 mm<sup>2</sup>) micro-inductor in a PwrSoC (Power system on Chip), based on the hybrid integration on silicon substrate of fully sintered ferrite cores with windings made from electroplated copper. This article presents the full characterization of low-profile ferrite cores with a focus on losses in the range of frequency of interest (above 1 MHz). Four materials are compared: cores either cut from commercial films or screen printed from an in-house made paste. We believe that this approach presents a low-cost solution due to minimum number of fabrication steps and high throughput deposition techniques: electroplating for copper windings and screen printing or milling for cores.

After developing target specifications based on realistic applications and after proposing a preliminary design for the micro-inductors, section 3 presents the fabrication processes for realizing ferrite cores and test micro-inductors. In the last section, results of magnetic and electrical characterization are presented in details for the four materials, with B-H curves, complex permeability, inductance performance and core losses. The effect of sintering temperature on the performance is eventually discussed.

## 2. Specifications, material choices and design

In order to achieve an integration of the inductor with high specific inductance, while keeping low losses, frequencies in the MHz range are selected. The specifications, defined according to typical commercial inductors, are the following: an inductance in the range of 200-1000 nH, an equivalent series resistance in the range of 0.1Ω - 0.2 Ω at bias current of 0.6 A and operating at 6 MHz. In the objective of evaluating performance prior to inductor fabrication, several NiZn ferrites were selected among which:

- Commercial ferrite films by ESL ElectroScience [31,32]: ESL 40010® and ESL40011® with expected permeabilities of 60 and 200 respectively. These materials were characterized at macro-scale by Mu et al [24]. At 1.5 MHz and 20 mT, losses of 1000 mW.cm<sup>-3</sup> and 2000 mW.cm<sup>-3</sup> were measured for 40010 and 40011.
- In-house made ferrite powders, namely U70 and U200 based on ref. [33] that will be mixed into a paste for screen printing deposition. Selected ferrites are NiZnCuCo with a ratio of Ni/Zn fixed to a value of 0.55 for U70 and 0.43 for U200: the smaller the ratio of Ni/Zn the higher the permeability of ferrite according to previous work [33]. Cobalt was added 3.5 at% in selected ferrites in order to increase the cut-off frequency and decrease losses: 200 mW.cm<sup>-3</sup> at 1.5 MHz under 25 mT were reported.

The simplest micro-inductor topology in terms of core fabrication is a thin film ferrite in a rectangular shape wrapped by multi-level metal windings as shown in figure 1. The total thickness of the micro-inductor should be less than 250 μm to constitute a competitive solution in comparison to current commercial inductors, for example

LPS3010 inductor by Coilcraft [34]. To avoid difficulties in fabrication, the thickness of copper windings is fixed to 50  $\mu\text{m}$ . In the design, the final realized micro-inductor will have the winding forming by bottom copper tracks, vias and top copper tracks (see figure 1). Hence, the magnetic core is limited to a thickness of 150  $\mu\text{m}$ .

Based on target specifications of the inductor, the design was made by adjusting parameters of the core and winding dimensions. The geometrical input parameters are: core width ( $X$ ), core length ( $Y$ ), magnetic core width ( $w$ ), magnetic core thickness ( $t$ ), thickness and width of copper wire and number of turns ( $N$ ). The output parameters are the DC and AC resistance, the total inductance and maximum magnetic induction. Design was done by Excel with analytical expressions. In the constrained dimension, the combination of  $X$ ,  $Y$ ,  $w$  and  $N$  that give the best output of total inductances, DC and AC resistances was selected for the test inductor. We have checked that with  $B_{\text{sat}}$  about 0.25T, the inductors would operate normally at 0.6A DC and reach specifications. This preliminary design is necessary to define realistic core dimensions, i.e. close to optimized version. Defined dimensions for full inductors are 1.54 x 2.64 mm<sup>2</sup> with the magnetic core width of 350  $\mu\text{m}$ ; these cores will be integrated in the micro-inductor with 21 turns of winding. Permeability and core loss density characterization of the developed ferrite materials shaped in the chosen dimensions will be carried out. Eventually, future design optimization will include these magnetic properties.

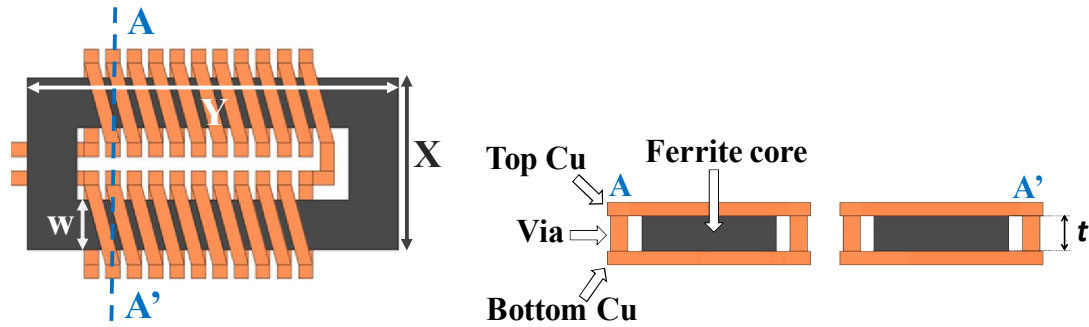


**Figure 1.** Schematic design of proposed final micro-inductors with top-view and cross section

### 3. Experimental

We propose two approaches for the fabrication of ferrite cores according to their nature:

- From commercial ferrite films: ESL 40010® and ESL 40011® which will be named 40010 and 40011 respectively in the rest of the article. Two layers of thin film ferrite about 70  $\mu\text{m}$  each were bonded together by applying a pressure of 800 N/cm<sup>2</sup> in 10 minutes at 90°C under vacuum of 10<sup>-3</sup> mbar in a wafer bonding machine AML AWB04. The double-layer films (140  $\mu\text{m}$  thick) were then cut by a micro-milling machine Réalméca RV2 SP (200  $\mu\text{m}$  end mill); the cutting dimensions were adjusted for shrinkage occurring during the sintering phase of these materials.
- From the in-house ferrite powder: synthesized NiZn ferrite powder was mixed with organics including binders, plasticizers, and dispersants provided by ESL® to form magnetic slurry. Dry film photo-resists were used to form 190 $\mu\text{m}$ -thick moulds on Kapton® polyimide substrates by photolithography technique. The ferrite paste

was then filled into the mould by screen printing technique using DEK Horizon 01i equipment, followed by thirty minutes vacuum treatment to degas the paste via a mechanical rotary pump. The ferrite composite was dried at 110°C for ten minutes and then collected manually after the photo-resist was removed.

Sintering temperature of each ferrite was determined after the shrinkage peaks were identified by thermomechanical analysis using Setsys Evolution TMA. Based on TMA curves, the milled cores were sintered at 885°C and 950°C under flux of oxygen during 3 and 2 hours respectively. The printed cores were sintered at 980°C during 2 hours. The footprint of cut and printed cores after sintering is about 1.2x2.6 mm<sup>2</sup>. Core thicknesses were measured after sintering: for milled cores, thickness ranges between 108 – 110 µm; for printed cores thickness ranges between 90 and 105 µm. Microstructures of cores were observed by scanning electron microscopy Hitachi S4800. Compositions of different ferrites were estimated by energy dispersive analysis (EDS). The magnetic properties of thin film ferrites were characterized by a vibrating sample magnetometer Versalab™ - 3 Tesla Cryogen-free from Quantum Design. To extract the complex permeability ( $\mu'$  and  $\mu''$ ) of the used ferrite materials, toro-shape samples were also prepared and measured in a magnetic material test fixture Agilent 16454A on an impedance analyzer Agilent 4294A. The dimension of toro samples was selected according to the sizes of the fixture holders in the test kit. Toros of ESL ferrite films have the internal diameter of 4 mm, the external diameter of 6 mm and the thickness of 108 µm. Toros of U70 and U200 home-made ferrites have dimension of 5 mm, 14 mm and 1.5 mm as internal diameter, external diameter and thickness.

Eventually, in order to extract magnetic properties such as inductance and core losses, test inductors were fabricated: 50 µm thick copper bottom tracks are deposited on Si/SiO<sub>2</sub>/Ti/Au wafer by photolithography and electroplating. The seed layer is removed after electroplating by wet etching in potassium iodide solution KI+I<sub>2</sub> and HF acid. For test inductors, ground-signal-ground contact pads and a ground ring around the inductor are created in order to test the device under RF probes. Sintered ferrite cores are placed on Cu tracks and gold 25µm-diameter micro-wires are bonded by ball wire bonding technique to complete the winding.

Figure 2 shows a ferrite core after sintering and a test inductor with wire-bonds. These test inductors were characterized by an impedance analyzer (Agilent 4294) to determine the inductance versus frequency and versus DC bias and on a LCR meter (Agilent 4284A) to extract core losses versus AC current (rms).

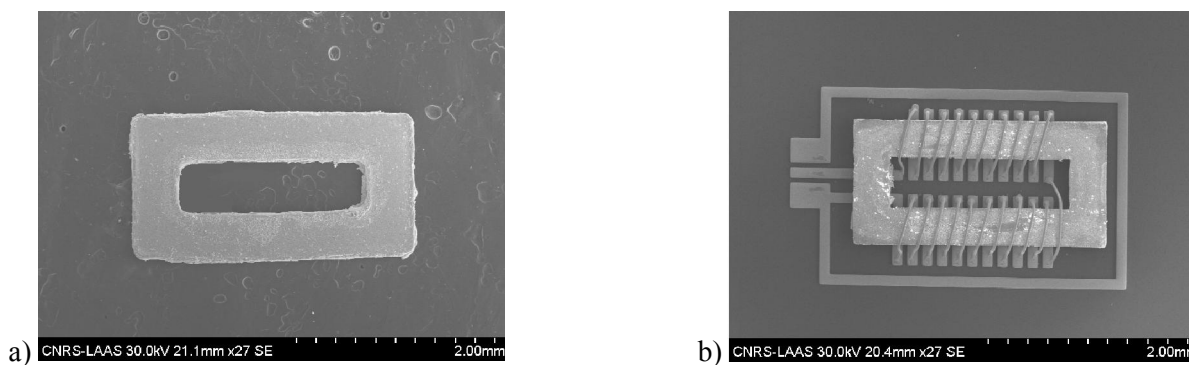


**Figure 2.** (a) Microscope image of ESL® thin-film milled cores after sintering and (b) SEM image (top view) of the test inductor with printed core and with wire-bonds to complete magnetic circuits.

## 4. Results and discussion

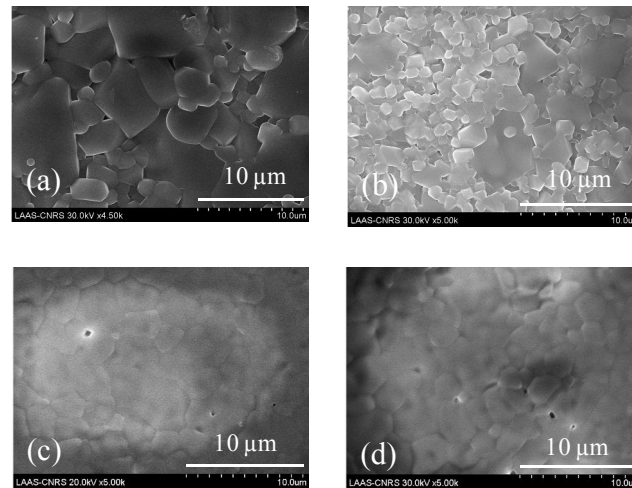
### 4.1 Magnetic material characterization

Figure 3 shows the microstructure of different ferrites after sintering. The grains of thin-film 40010 and 40011 have a bimodal distribution, with large grains of 5-8  $\mu\text{m}$ , covering around 50% of the volume, and small grains of 2-3  $\mu\text{m}$  in diameter. Grain sizes of printed ferrite U70 and U200 are in the range of 1.5-6  $\mu\text{m}$ . For all cores, the shrinkage was measured to be 15-20% with no cracks. The compositions of these ferrites are listed in table 1.

The B-H characteristics of ferrites are presented in figure 4. The measured samples are free-standing, about 110  $\mu\text{m}$  thick in a square dimension of 2x2  $\text{mm}^2$ . The induction saturation is in the range of 0.25-0.30 T, with a coercive field of 0.8-5.8 Oe (or 53-462 A/m). 40010 exhibits the highest coercive field which is due to the highest amount of magnetic phase (Ni and Fe) in 40010 ferrite compared to other ferrites ; a similar effect was observed when doing some copper substitution into Ni-Zn ferrites [35]. Magnetic remanences are 0.8-8% of the saturation magnetization.

**Table 1:** Composition of different ferrites estimated by SEM-EDS

Ferrite	Composition
40010 (Ni/Zn = 1.49)	$\text{Ni}_{0.49}\text{Zn}_{0.33}\text{Cu}_{0.18}\text{Fe}_2\text{O}_4$
40011 (Ni/Zn = 0.47)	$\text{Ni}_{0.28}\text{Zn}_{0.60}\text{Cu}_{0.12}\text{Fe}_2\text{O}_4$
U70 ( Ni/Zn = 0.55, Co = 0.035)	$(\text{Ni}_{0.30}\text{Zn}_{0.55}\text{Cu}_{0.15})_{0.965}\text{Co}_{0.035}\text{Fe}_2\text{O}_4$
U200 ( Ni/Zn = 0.43, Co = 0.035 )	$(\text{Ni}_{0.24}\text{Zn}_{0.56}\text{Cu}_{0.20})_{0.965}\text{Co}_{0.035}\text{Fe}_2\text{O}_4$



**Figure 3.** SEM images of ferrite microstructure for (a) 40010 sintered at 950°C/2hours and (b) 40011 sintered at 885°C/3hours, (c) (d) U70 and U200 sintered at 980°C/2hours

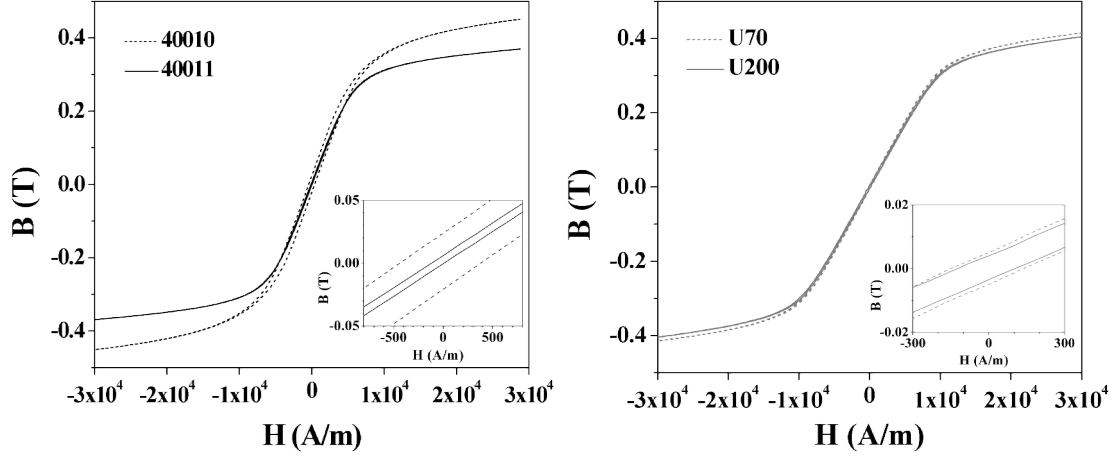


Figure 4. B-H curves of thin film ferrite measured by VSM

#### 4.2 Electrical characterization

The complex permeability of each material (40010, 40011, U70 and U200) was extracted as a function of frequency (as shown in figure 5) from impedance measurements of ferrite tores mounted on the magnetic test fixture using the following equation:

$$\mu_r^* = \frac{2\pi(Z_m^* - Z_{sm}^*)}{j\omega\mu_0 h \ln \frac{c}{b}} + 1 \quad (1)$$

in which  $Z_m^*$  is the impedance of the test fixture with the tore and  $Z_{sm}^*$  is the impedance of the test fixture without the tore;  $\omega$  is measurement pulsation  $\omega = 2\pi f$ ,  $\mu_0$  is permeability of free space,  $h$  is thickness of the tore;  $c$  and  $b$  are external and internal diameter of the tore respectively.

40011 ferrite presents a permeability of 200 stable up-to 10 MHz while that value for 40010 is 60 and stable until 70 MHz. These measured values correspond to values provided by ESL. The secondary permeability of 40010 at zero DC and small AC signal is small up-to 50 MHz, whereas that of 40011 increases quickly from 1-3 MHz. Higher secondary permeability ( $\mu''$ ) means higher losses. U70 and U200 have permeabilities of 86 and 190 stable up to 50 MHz and 10 MHz respectively. When comparing U200 with 40011 films at 6 MHz, which is the frequency of interest: both show high primary permeability. However, secondary permeability for 40011 films is much higher than U200 film. We thus expect higher core loss density for 40011 than for U200 under the same operating conditions. Losses of U200 ferrite are small thanks to the cobalt contribution, as reported by Lucas [33]. Table 2 summarizes magnetic properties of selected ferrites.

Table 2: Magnetic properties of different ferrites

	40011	40010	U200	U70
Permeability $\mu'$	200	60	190	86
Induction saturation $B_s$ (T)	0.25	0.30	0.25	0.25
Coercive field $H_c$ (Oe)	0.8	5.8	1.5	1.9
Resonance frequency $F_{res}$ (MHz)	30	100	30	100

Electrical characterizations were performed for different magnetic cores with 21-turn coil. Figure 6 a) shows the inductance of test inductors as a function of frequency. An inductance as high as 860 nH corresponding to 215 nH.mm<sup>-2</sup> was obtained for the 40011 core and 287 nH corresponding to 72 nH.mm<sup>-2</sup> obtained for 40010 cores at 6 MHz while the air core inductor has only an inductance of 18 nH.

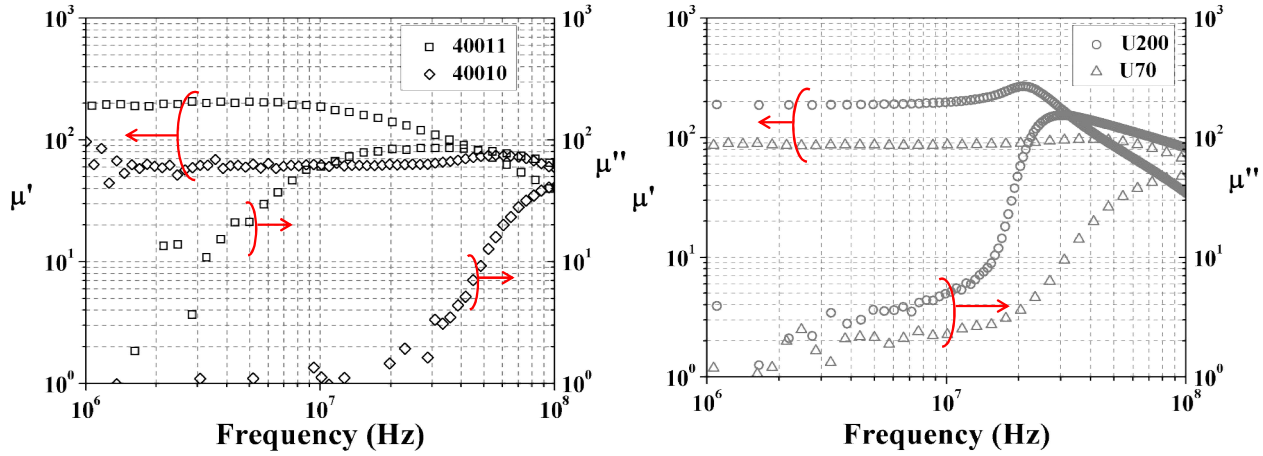


**Figure 5.** Measured complex permeability: ESL 40010® and 40011® ferrites sintered at 950°C/2h and 885°C/3h (b=4 mm, c=6 mm and h= 108 μm), U70 and U200 home-made ferrites sintered at 980°/2h (b=5 mm, c=14 mm and h=1.5 mm)

These fully sintered ferrite cores offering high values of inductance density as demonstrated with the test inductors present thus a real advantage for realizing small rectangular micro-inductors on chips compared to other reported non-sintered ferrite inductors [8,26,28]. Figure 6 b) shows the inductance versus superimposing DC bias current for the four films. The inductance drops quite rapidly, especially for 40011 and U200 ferrites. This is due to the non-linearity of the permeability versus DC magnetic field. The decrease of μ versus pre-magnetization field was already observed by Mu et al [24]. The higher the permeability, the more severe is the drop. This behavior is a major drawback and it will have to be taken into account in the design optimization of micro-inductors. Meanwhile, 40010 cores have permeability more stable with DC bias current, yet they have lower permeability (see figure 5 a) and figure 6 b)).

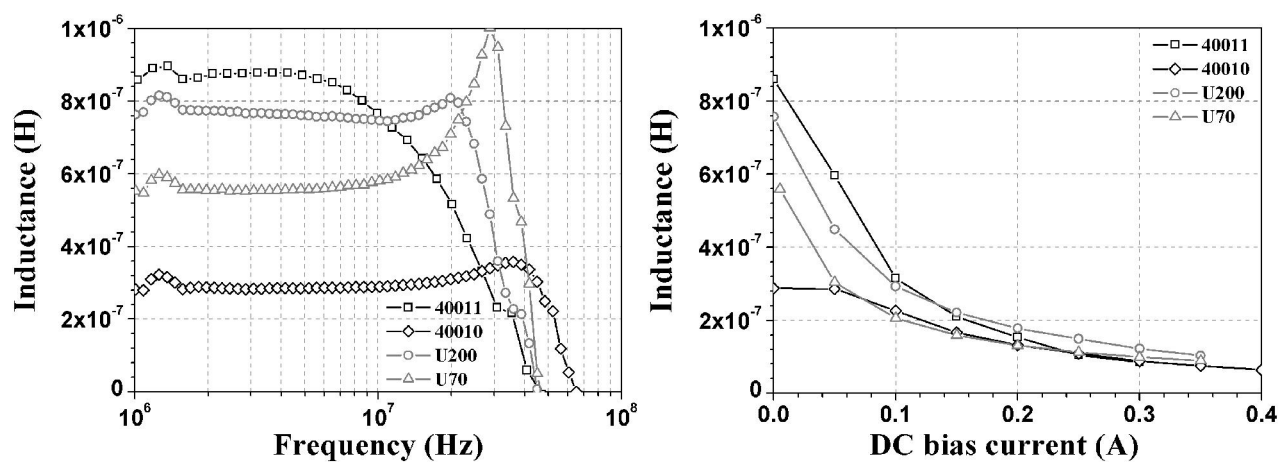


**Figure 6.** Measured inductance of the test inductors made of different cores as functions of a) frequency and b) bias current at 6 MHz

### 4.3. Core losses

For design purposes, it is important to extract core losses at different excitation conditions: AC, DC and frequency. In soft ferrite films, core losses include eddy current losses, hysteresis losses and residual losses. The total core losses per unit volume were extracted from under-probe measurements of test inductors with varying sine-wave signal using equation (2):

$$P_v = \frac{R_s I_{AC}^2}{A_e l_e} \quad (2)$$

$R_s$  is obtained by subtracting the resistance of air-core inductor from the resistance of magnetic-core inductor.  $I_{AC}$  is the alternating current (rms),  $A_e$  is the effective magnetic cross section and  $l_e$  is the mean magnetic length.

Figure 7 shows extracted core losses versus frequency for the 40011 film. Measurement is carried out at different levels of sine wave signal  $I_{AC}$  (rms). The induction variation is referred from AC current by Eq. (3) in which  $L_s$  is the difference of impedance's imaginary parts from magnetic-core inductor and air-core inductor divided by the measurement pulsation  $\omega$ . As expected, losses increase with frequency and with sine wave amplitude.

$$B_{AC} = \frac{L_s * I_{AC}}{N * A_e} \quad (3)$$

Analytical models of core losses were generated by fitting the datasheet curve  $P_v$  in the range of 1-10MHz using Steinmetz equation (4) with a least squares method [36,37]. Steinmetz equation works well for ferrite losses with sine-wave signal (see fitting in figure 7). Similar curves were produced for the three other materials. Table 3 summarizes the parameters  $k$ ,  $\alpha$  and  $\beta$  of four materials for the frequency range 1-10 MHz and at zero DC bias.

$$P_v = k * f^\alpha * B_{AC}^\beta \quad (4)$$

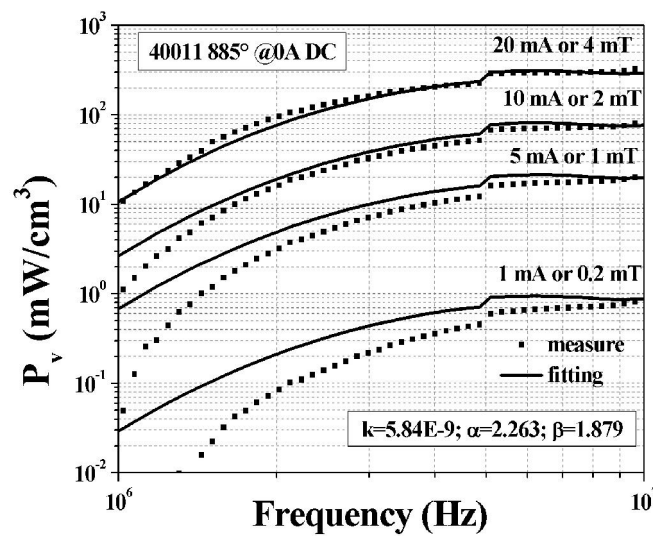
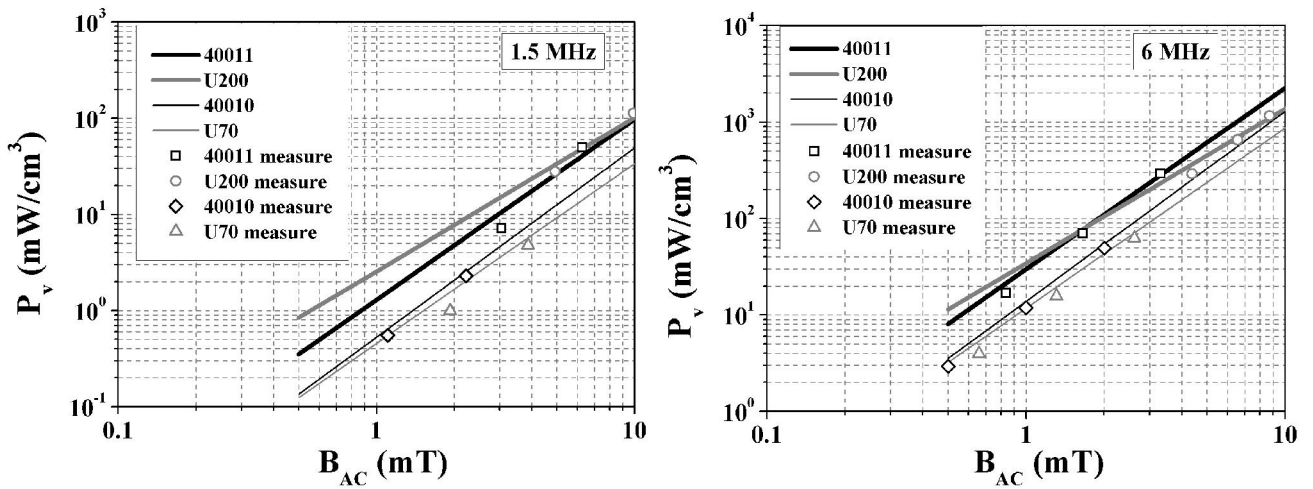


Figure 7. Measured and analytical core losses versus frequency for 40011 films

**Table 3:** Values of parameters  $k$ ,  $\alpha$  and  $\beta$  obtained for four materials at zero DC bias, apply for frequency 1-10 MHz and  $B_{AC} = 0.1-10\text{mT}$

Ferrites	$k$	$\alpha$	$\beta$
40011	5.84E-09	2.263	1.879
40010	1.199E-09	2.356	1.969
U200	4.084E-07	1.878	1.601
U70	6.049E-10	2.345	1.869

For comparison purposes, core losses of the four studied materials versus magnetic induction, at two frequencies (1.5 and 6 MHz) are presented in figure 8. These curves were generated from analytical loss models: experimental data points are also shown. 40010 and U70 cores show the smallest losses. As shown in figure 7, 40011 core exhibits losses about  $300 \text{ mW}\cdot\text{cm}^{-3}$  at 4 mT and 5 MHz, comparable with the reported value of  $400 \text{ mW}\cdot\text{cm}^{-3}$  for the same conditions by Mu et al. [24]. At 10 mT, U200 core presents lower losses than 40011: about  $100 \text{ mW}\cdot\text{cm}^{-3}$  at 1.5 MHz which is in the range of already reported results for this material by Lucas, i.e.  $200 \text{ mW}\cdot\text{cm}^{-3}$  at 25 mT [33]. At 6 MHz, all losses increase by a factor of 30: at induction value of 10 mT, losses reach levels of  $1500-2500 \text{ mW}\cdot\text{cm}^{-3}$  for U200 and 40011 ferrites.



**Figure 8.** Core losses of four materials as a function of induction variation at 1.5 MHz and 6 MHz

#### 4.4. Effect of sintering temperature

The choice of sintering temperature for ferrites is based on the TMA curves. As shown figure 9, the solid state reactions happen from  $850^\circ\text{C}$  to  $950^\circ\text{C}$  for 40011. The sintering temperature should fall in this range. In this work, we give the comparison for two sintering temperatures  $885^\circ$  and  $950^\circ$ . The effect of sintering temperature on the properties of 40011 ferrite was studied.

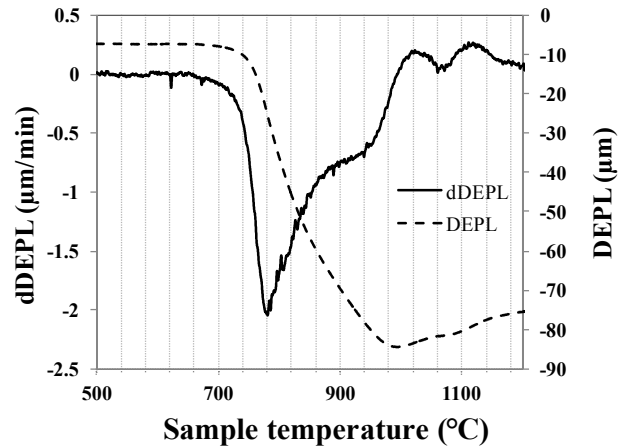


**Figure 9.** Thermomechanical analysis of 40011 ferrite; DEPL is the displacement of the sample, dDEPL is the derivative of the displacement.

It is shown that sintering at higher temperature makes the micro-structure of ferrites coarser. Bigger grains are formed at higher sintering temperature (see figure 10). Concerning magnetic properties, higher sintering temperature brings higher permeability. 40011 cores show a permeability of 300 for sintering temperature of 950°C and 200 for sintering temperature of 885°C (see figure 11). This phenomenon can be explained by Globus model [38]: at low induction condition, domain wall bulging, instead of domain wall displacement, is responsible for  $\mu'$ . According to this model,  $\mu'$  increases with the increasing distance between pinned edges of domain wall, which is approximately equal to grain size. However, the disadvantages are: the cores sintered at higher temperature have higher losses and a lower cut-off frequency (see figure 12 and 11). Core losses include hysteresis loss, eddy current loss and residual loss in which eddy current loss is considered negligible because of the high resistivity of selected ferrites. Under low induction condition, the hysteresis loss is smaller for smaller grain size [39]. Hence, total core losses are smaller for 40011 sintered at 885°C compared to 950°C. Magnetic properties and extracted loss coefficients of 40011 cores are presented in table 4 and table 5.

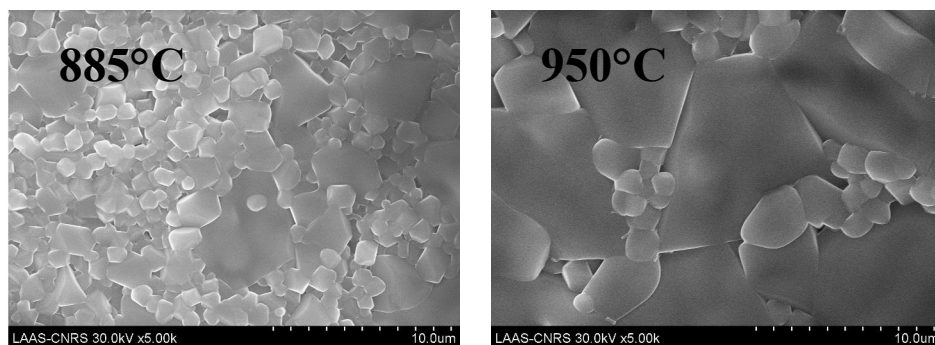


**Figure 10.** Effect of sintering temperature on microstructure of 40011 ferrite

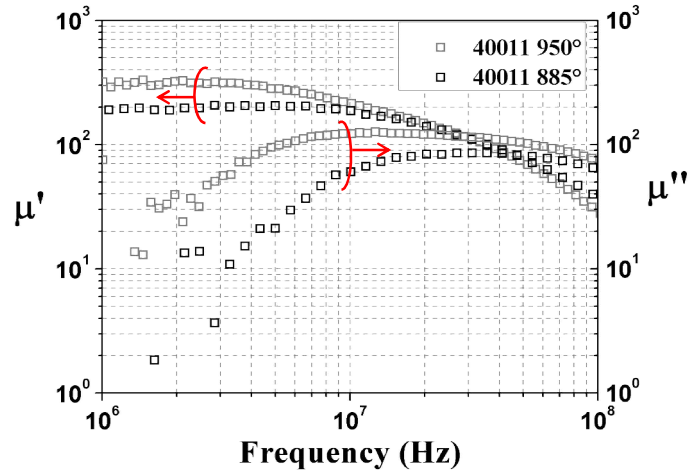


**Figure 11.** Complex permeability of 40011 cores sintered at different temperature

**Table 4:** Magnetic properties of 40011 sintered at different temperature

40011	885°C	950°C
Permeability $\mu'$	200	300
Induction saturation $B_s$ (T)	0.25	0.25
Coercive field $H_c$ (Oe)	0.8	1.9
Resonance frequency $F_{res}$ (MHz)	30	10

**Table 5:** Loss coefficients at zero DC bias for 40011 cores sintered at two temperatures fitted with Eq. 4, apply for frequency 1-10 MHz and  $B_{AC} = 0.1-10$  mT. (Measurement results not shown here).

Ferrites	k	$\alpha$	$\beta$
40011 885°C	5.84E-09	2.263	1.879
40011 950°C	2.438E-08	2.226	1.89

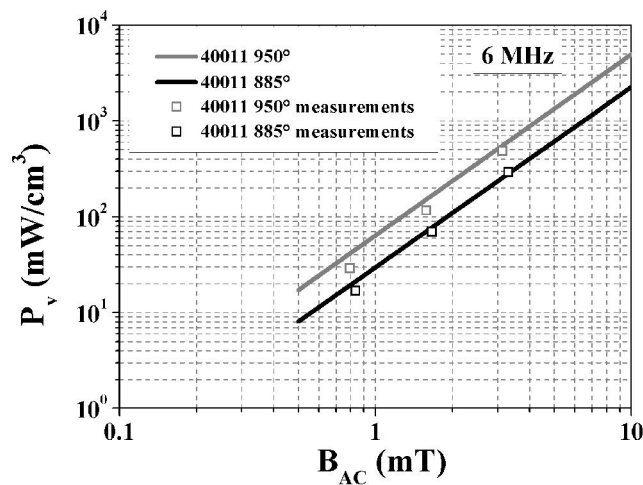


**Figure 12.** Losses of 40011 cores sintered at different temperature

## 5. Conclusions and perspectives

Ferrite-based rectangular cores were fabricated via two techniques: screen printing and milling of commercial green tape films and their performance evaluated. Chosen ferrites are very interesting in terms of permeability. Test inductors containing these ferrite cores achieve a very high inductance density above already reported micro ferrite inductors thanks to the pre-eminent magnetic properties of fully sintered ferrite. In this work, it was shown that at 6 MHz, 215 nH.mm<sup>-2</sup> of inductance could be reached for test inductors including 40011 cores and 72 nH.mm<sup>-2</sup> for the ones including 40010 cores. However, when superimposing a DC bias current, all four materials chosen for core fabrication exhibit a large decrease of permeability, which is a potential disadvantage of these soft ferrite cores for high DC current application. In term of losses, 40010 and U70 have the smallest losses about 1 W.cm<sup>-3</sup> at 6 MHz under 10 mT. U200 and 40011 losses range between 1.5 and 2.5 W.cm<sup>-3</sup> respectively under the same conditions; U200 and 40011 ferrites could be chosen when high inductance density is desired for the micro-inductor. Further work is needed to measure losses and extract corresponding models for higher induction levels and for additional static magnetic fields. Optimization for design of future micro-inductors including these ferrite films is to be done with the consideration of the losses models developed. Final micro-inductors will be realized by thick photo-resist method to insulate ferrite cores and deposit copper tracks on top. X-ray characterization will be carried out to give information regarding the structure of materials. Dielectric constants will be measured at different frequencies to study the capacitive character of these ferrites.

## Acknowledgement

This work was funded by PRIIM project using micro fabrication platform at LAAS (supported by French RENATECH network) and 3DPhi platform at LAPLACE. VSM measurements were done at ONERA and CIRIMAT (Toulouse, France): we thus kindly thank Isabelle Séguy, Matthieu Palosse, Le Trong Hoa and M. Gougeon for performing the measurements. We would like also to thank Frédéric Voiron from IPDIA and Jean-Philippe Michel from CEA-Léti for fruitful discussions on the subject during PRIIM project. Thanks to ESL ElectroScience for providing us samples of ESL 40011® and ESL 40010® films.

## References

- [1] Wang N, O'Sullivan E J, Herget P, Rajendran B, Krupp L E, Romankiw L T, Webb B C, Fontana R, Duch E A, Joseph E A, Brown S L, Hu X, Decad G M, Sturcken N, Shepard K L and Gallagher W J 2012 Integrated on-chip inductors with electroplated magnetic yokes (invited) *Journal of Applied Physics* **111** 07E732
- [2] Lu S, Sun Y, Goldbeck M, Zimmanck D R, Sullivan C R 2007 30-MHz power inductor using nano-granular magnetic material. In: *38th IEEE Power Electronic Specialists Conference*, Orlando, FL 1773–6
- [3] Flynn D and Desmulliez M P Y 2009 Design, Fabrication, and Characterization of Flip-Chip Bonded Microinductors *IEEE Transactions on Magnetics* **45** 3055-63
- [4] Kowase I, Sato T, Yamasawa K and Miura Y 2005 A planar inductor using Mn-Zn ferrite/polyimide composite thick film for low-voltage and large-current DC-DC converter *IEEE Transactions on Magnetics* **41** 3991-3
- [5] Lee D W, Hwang K-P and Wang S X 2008 Fabrication and Analysis of High-Performance Integrated Solenoid Inductor With Magnetic Core *IEEE Transactions on Magnetics* **44** 4089-95
- [6] Wang N, O'Donnell T, Roy S, McCloskey P and O'Mathuna C 2007 Micro-inductors integrated on silicon for power supply on chip *Journal of Magnetism and Magnetic Materials* **316** E233-E7
- [7] Mathuna C O, Wang N, Kulkarni S and Roy S 2012 Review of Integrated Magnetics for Power Supply on Chip (PwrSoC) *IEEE Transactions on Power Electronics* **27** 4799- 816
- [8] Fukuda Y, Inoue T, Mizoguchi T, Yatabe S and Tachi Y 2003 Planar inductor with ferrite layers for DC-DC converter *IEEE Transactions on Magnetics* **39** 2057-61

- [9] Meyer C D, Bedair S S, Morgan B C and Arnold D P 2012 Influence of Layer Thickness on the Performance of Stacked Thick-Film Copper Air-Core Power Inductors *IEEE Transactions on Magnetics* **48** 4436 - 9
- [10] Jia H, Lu J, Wang X, Padmanabhan K and Shen Z J 2011 Integration of a Monolithic Buck Converter Power IC and Bondwire Inductors With Ferrite Epoxy Glob Cores *IEEE Transactions on Power Electronics* **26** 1627-30
- [11] Liakopoulos T, Panda A, Wilkowski M, Lotfi A, Tan K H, Zhang L, Lai C and Chen D 2012 Introducing FCA, a New Alloy for Power Systems on a Chip and Wafer Level Magnetic Applications *13th International Conference on Electronic Packaging Technology & High Density Packaging (Icept-Hdp 2012)* 948-53
- [12] Kim J, Kim M, Herrault F, Park J and Allen M G 2013 Highly Laminated Soft Magnetic Electroplated CoNiFe Thick Films *IEEE Magnetics Letters* **4** 5000204
- [13] Lee J, Hong Y K, Bae S, Jalli J, Park J, Abo G S, Donohoe G W and Choi B C 2011 Integrated Ferrite Film Inductor for Power System-on-Chip (PowerSoC) Smart Phone Applications *IEEE Transactions on Magnetics* **47** 304-307
- [14] Harburg D V, Khan G R, Herrault F, Kim J, Levey C G and Sullivan C R 2013 On-chip RF power inductors with nanogranular magnetic cores using prism-assisted UV-LED lithography *Solid-State Sensors, Actuators and Microsystems, 2013 Transducers & Eurosensors XXVII: The 17th International Conference (IEEE, Barcelona, 2013)* 701-4
- [15] Yu X, Kim J, Herrault F and Allen M G 2014 Silicon-embedded toroidal inductors with magnetic cores: Design methodology and experimental validation *Applied Power Electronics Conference and Exposition (APEC), 29th Annual (IEEE, Fort Worth, TX)* 763-7
- [16] Lee F C, and Li Q 2013 High-Frequency Integrated Point-of-Load Converters: Overview *IEEE Transactions on Power Electronics* **28** 4127-36
- [17] Harburg D V, Hanson A J, Yue S, Qui J, Tian R, Christopher G L, Charles R S and David O 2013 Measured performance and micro-fabrication of racetrack power inductors *Energy Conversion Congress and Exposition (ECCE) 2013 (IEEE, Denver, CO)* 614-20
- [18] Meere R, Wang N, O'Donnell T, Kulkarni S, Roy S, and O'Mathuna S C 2011 Magnetic-Core and Air-Core Inductors on Silicon: A Performance Comparison up to 100 MHz *IEEE Transactions on Magnetics* **47** 4429-32
- [19] Kim J, Kim J K, Kim M, Herrault F and Allen M G 2013 Microfabrication of toroidal inductors integrated with nanolaminated ferromagnetic metallic cores *Journal of Micromechanics and Microengineering* **23** 114006
- [20] Sugawa Y, Ishidate K, Sonehara M and Sato T 2013 Carbonyl-Iron/Epoxy Composite Magnetic Core for Planar Power Inductor Used in Package-Level Power Grid *IEEE Transactions on Magnetics* **49** 4172-5
- [21] Bharadwaj S, Ramesh T and Murthy S R 2013 Fabrication of microinductor using Nanocrystalline NiCuZn ferrites *Journal of Electroceramics* **31** 81-7
- [22] Mu M, Zhang W, Lee F C and Su Y 2013 Laminated low temperature co-fired ceramic ferrite materials and the applications for high current POL converters *Energy Conversion Congress and Exposition (ECCE) (IEEE, Denver, CO)* 621-7
- [23] Zhang W, Su Y, Mu M, Gilham D J, Li Q and Lee F C 2014 High Density Integration of High Frequency High Current Point-of-Load (POL) Modules with Planar Inductors *IEEE Transactions on Power Electronics* pp 1
- [24] Mu M, Su Y, Li Q, Lee F C 2011 Magnetic Characterization of Low Temperature Co-fired Ceramic (LTCC) Ferrite Materials for High Frequency Power Converters *2011 IEEE Energy Conversion Congress and Exposition (ECCE)* 2133-8
- [25] Bae S, Hong Y K, Lee J J, Jalli J, Abo G S, Lyle A, Choi B C and Donohoe G W 2009 High Q Ni-Zn-Cu Ferrite Inductor for On-Chip Power Module *IEEE Transactions on Magnetics* **45** 4773-6
- [26] Bang D H and Park J Y 2009 Ni-Zn Ferrite Screen Printed Power Inductors for Compact DC-DC Power Converter Applications *IEEE Transactions on Magnetics* **45** 2762-5
- [27] Fang X, Wu R, Peng L and Sin J K O 2013 A Novel Silicon-Embedded Toroidal Power Inductor With Magnetic Core *IEEE Electron Device Letters* **34** 292-4
- [28] Wang M L, Li J P, Ngo K D T and Xie H K 2011 A Surface-Mountable Microfabricated Power Inductor in Silicon for Ultracompact Power Supplies *IEEE Transactions on Power Electronics* **26** 1310-5
- [29] Nguyen Y M, Brunet M, Laur J P, Bourrier D, Charlot S, Valdez-Nava Z, Bley V and Combettes C 2013 Low-profile small-size ferrite cores for powerSiP integrated inductors *Power Electronics and Applications (EPE), 15th European Conference (IEEE, Lille)* pp 1-7
- [30] Nguyen Y M, Brunet M, Laur J P, Bourrier D, Charlot S, Valdez-Nava Z, Bley V and Combettes C 2013 Soft ferrite cores characterization for integrated micro-inductors *13th International Conference on Micro- and Nano-Technology for Power Generation and Energy Conversion Applications (PowerMEMS) Imperial Coll London, London, England, J. Phys.: Conf. Ser.* **476** 012139
- [31] ESL 40010® datasheet
- [32] ESL 40011® datasheet
- [33] Lucas A 2012 Etude et mise au point de transformateurs large bande radiofréquence. In: *L'Ecole normale supérieure de Cachan, (ENS Cachan/CNRS/UMR 8029: L'Ecole normale supérieure de Cachan)*
- [34] LPS3010 inductor by Coilcraft <http://www.coilcraft.com/lps3010.cfm>
- [35] Caltun F O, Spinu L and Stancu A 2001 Magnetic properties of high frequency Ni-Zn ferrites doped with CuO *IEEE Transactions on Magnetics* **37** 2353-5
- [36] Sullivan C R 2012 Overview of core loss prediction for non-sinusoidal waveforms. In: *APEC: Dartmouth Magnetic Components and Power Electronics Research Group*
- [37] Havez L 2013 3D Power Inductor: Calculation of Iron Core Losses. ed Y L E. Sarraute Proceedings of the 2013 COMSOL conference in Rotterdam
- [38] Globus A 1977 Some physical considerations about domain-wall size theory of magnetization mechanisms *Journal De Physique* **38** 1-15
- [39] Kondo K, Chiba T, and Yamada S 2003 Effect of microstructure on magnetic properties of Ni-Zn ferrites *Journal of Magnetism and Magnetic Materials* **254** 541-3